Small angle neutron scattering studies of HbA in concentrated solutions

S. Krueger,* S.-H. Chen,‡ J. Hofrichter,§ and R. Nossal§

*University of Maryland, College Park, Maryland 20742; ‡Massachusetts Institute of Technology, Cambridge, Massachusetts 02139; and §National Institutes of Health, Bethesda, Maryland 20892 USA

ABSTRACT Differential cross-sections for neutrons scattered by normal human hemoglobin have been determined over the range of concentrations from 2 to ~35 weight percent. Data are compared with structure factors calculated from models of monodisperse hard spheres interacting through a screened Coulomb potential. Good agreement is noted when the volume fraction η is adjusted during multivariate fitting of data, but the fitted value of η is always lower than expected from the known Hb concentration of the samples. Calculations of cross-sections for polydisperse scatterers suggest that the samples may contain oligomers of the fundamental tetrameric Hb molecule.

INTRODUCTION

Normal human hemoglobin (HbA) is a tetrameric protein with a molecular weight of 64.5 kD, containing two α and two β chains. The protein functions at extremely high concentrations (0.3–0.4 g/cc) in red cells, and there has been considerable interest in characterizing its physical state under such conditions. Many techniques have been applied to this problem, including osmotic pressure (1), sedimentation equilibrium (2, 3), viscosity (4), and diffusion measurements (5–7). These experiments have been successfully interpreted using a model of monodisperse spheres interacting only by way of particle excluded volume (7–10).

Recent scattering studies suggest that appreciable amounts of associated hemoglobin exist within normal erythrocytes. For instance, values of Hb diffusion coefficients detected by microscope laser light scattering are lower than those expected for freely moving Hb monomers (11). Furthermore, if cell volume is decreased by varying the ionic strength of the suspension medium, the correlation time of forward-scattered photons increases, signifying the presence of yet larger scatterers (11). Also, small-angle neutron scattering (SANS) data from erythrocyte suspensions indicate possible HbA associations: when differential cross-section data are fitted to analytical structure factors calculated for monodisperse solutions, discrepancies are found between the fitted and anticipated values of the apparent volume fraction occupied by intracellular Hb (12). As is discussed below, a plausible explanation is that the measured cross-sections contain contributions arising from dimers and higher-order aggregates which scatter neutrons into smaller angles and thereby change the features of the scattering curves.

The interpretation of light scattering data from Hb within erythrocytes is subject to uncertainty, due to possible contributions of cell membranes and other cellular components to the observed signals (13). This is of less concern for SANS measurements because the scattering length of the suspension medium can be matched to that of the membranes, causing the latter to become essentially invisible to neutrons (12). Because differential scattering cross-sections are very sensitive to the structure of the scatterers, SANS can provide information on the state of aggregation of Hb molecules. However, extraction of such information in highly concentrated solutions is complicated by interparticle interference, and special procedures must be employed.

We report, here, on studies of various solutions of the CO derivative of purified HbA. Hemoglobin was studied near neutral pH at concentrations varying from 0.02 to 0.36 g/cc in D_2O. Data have been analyzed by a procedure which has been successfully applied to other biopolymer (14–16) and colloidal systems (17, 18), and the results qualitatively corroborate those obtained from erythrocyte suspensions (12). In particular, the scattering cross-sections can be fitted only by adjusting the volume fractions, $\{\eta\}$, to values significantly lower than those calculated from measured HbA concentrations. We demonstrate by computer simulations that this discrepancy can be explained by limited aggregation of hemoglobin tetramers.

S. Krueger's present address is National Institute of Standards and Technology, Gaithersburg, MD 20899.

EXPERIMENTAL PROCEDURES

Materials

Human HbO_2 initially was purified by DEAE-cellulose column chromatography (Whatman DE-52) of a freshly prepared lysate, and then divided into various aliquots. One portion was dialyzed against normal pH 7.4 Tris-NaCl buffer (0.1 M Tris, 0.1 M NaCl, 10^{-3} M EDTA) and then equilibrated with CO at a final Hb concentration of 0.116 g/cc. Another aliquot was extensively dialyzed against the same buffer which, however, was prepared in D_2O [pD = 7.4 = pH (meter reading) + 0.4] (19). A vacuum dialysis scheme was devised to concentrate the stock solution (final value, 0.356 g/cc), an aliquot of which then was stored under nitrogen as deoxy Hb, and the major portion equilibrated with CO. A concentration series of this sample was prepared by dilution into Tris-NaCl-D_2O buffer and equilibrated with CO. Hemoglobin concentrations were measured by diluting small aliquots of each sample into CO saturated, 0.05 M KH_2PO_4-NaOH buffer (pH 7.0). Optical densities were measured at 539 nM, using a Cary 17 spectrophotometer, and concentrations were determined by using an extinction coefficient of 14360 per heme.

A second concentration series was prepared by dialyzing a Hb stock solution against unbuffered D_2O to which a few drops of dilute NaOH had been added. Solutions of the stock were then made in CO equilibrated D_2O. The measured pD of a 0.241 g/cc solution of this material was pD 8.9. A third group of samples was prepared, without salt, to discern the effects of pH on intermolecular interactions. To do so, an aliquot of the pD 7.4 Tris-NaCl sample was dialyzed against pure D_2O, yielding a 0.247 g/cc Hb pD 7.2 sample. This sample then was mixed in various proportions with the corresponding pD = 8.9 sample, to provide additional unbuffered samples of pD 7.8 and pD 8.2. Finally, specimens for contrast variation measurements were prepared by mixing various amounts of ~0.02 g/cc Hb, pH 7.4, stock with ~0.02 g/cc Hb, pD 7.4, stock.

Neutron measurements

Differential cross-section data were acquired at the SANS spectrometer located at the National Institute of Standards and Technology (20). A beam of wavelength 5.5 Å and spread $\delta\lambda/\lambda \approx 25\%$ was used. Neutrons were collimated by using a coarse collimation configuration, consisting of an entrance pinhole of diameter 2.70 cm, a second pinhole of diameter 1.80 cm located at a distance of 450 cm from the first, and a third pinhole (mask) of diameter 1.27 cm located at the sample. The samples were contained in 1.0-mm path length cuvettes.

Scattered neutrons were detected with a 64 × 64 cm^2 position-sensitive detector of the Borkowski-Kopp type (21) which is divided into 128 × 128 pixels. Counts collected within each pixel were corrected for empty cell, background, and solvent incoherent scattering, normalized, and then radially averaged (22). The sample to detector distance was 360 cm so that, by setting the detector at an angle of 3.5°, the range of Bragg wave numbers, $Q = 4\pi\lambda^{-1} \sin(\theta/2)$, that could be accessed was $0.014 \leq Q \leq 0.168$ $Å^{-1}$. In some instances the data were put on an absolute scale by calibration against the scattering from a standard silica-gel sample. The scattering cross-section per unit sample volume is denoted as $I(Q)$.

DATA AND RESULTS

Differential scattering cross-sections, $I(Q)$, for a series of Hb CO solutions at pD 7.4, ranging in concentration from 0.02 g/cc to over 0.35 g/cc, are shown in Fig. 1. These data will be the focus of the discussion, because our major interest is in describing Hb near physiological pH. Because the pD of these samples is close to the isoelectric point, the Hb particles have only a small negative charge and do not sense each other until high concentrations are achieved. An interaction peak gradually emerges as the concentration increases, but the peak only becomes prominent at concentrations above 0.20 g/cc.

A second set of samples was studied under conditions chosen to accentuate the electrostatic interaction between particles. The conditions were pD 8.9 without added salt. In this case the HbCO molecules carry a much higher surface charge (~ −10 esu), and screening by solvent ions is minimized. Results are shown in Fig. 2. In these data the interaction peaks become prominent at solution concentrations as low as 0.05 g/cc, providing clear evidence

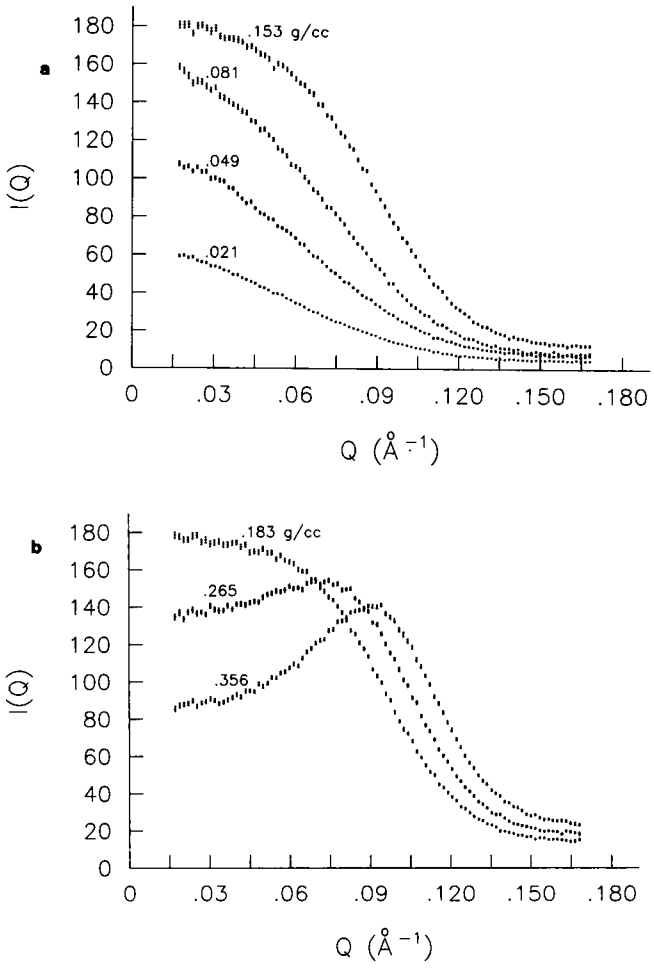

FIGURE 1. Concentration dependence of the differential neutron scattering cross-section for HbA in "physiological" D_2O buffer (pD 7.4, low molecular charge). C_{Hb} varies from 0.021 to 0.356 g/cc.

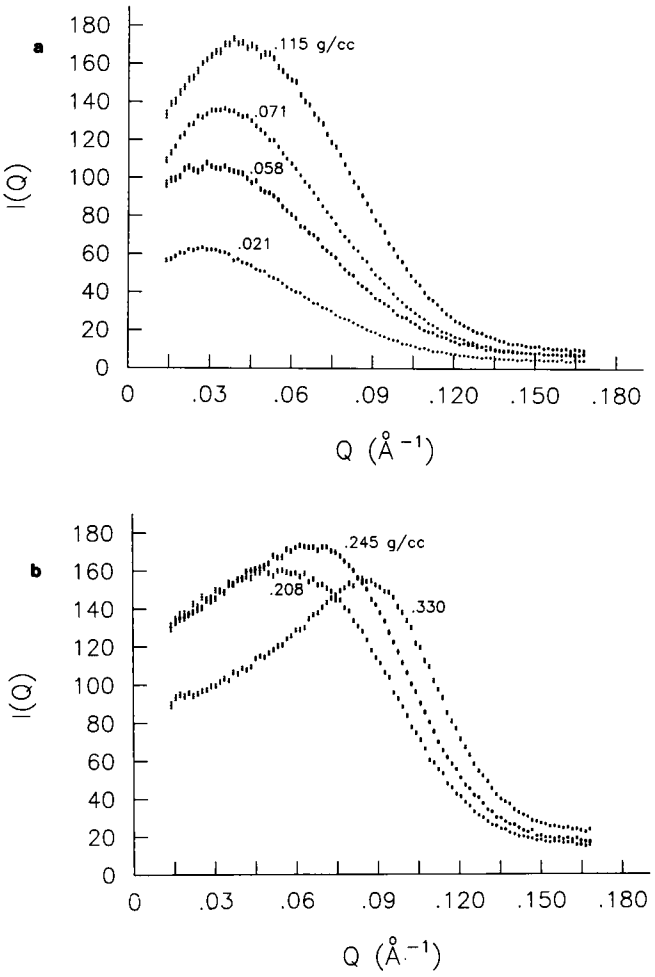

FIGURE 2. Concentration dependence of the differential neutron scattering cross-section for HbA in D_2O under conditions of high molecular charge (pD 8.9, nominal value). C_{Hb} varies from 0.021 to 0.330 g/cc.

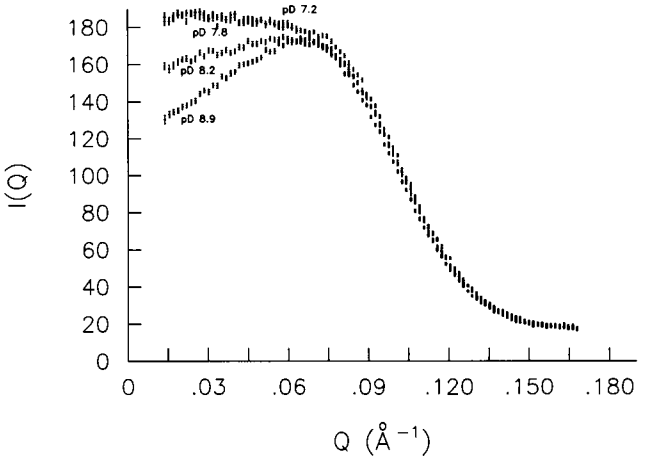

FIGURE 3. Differential neutron scattering cross-sections for concentrated Hb-D_2O samples of differing pD. C_{Hb} (pD 7.2) = 0.249 g/cc; C_{Hb} (pD 7.8) = 0.231 g/cc; C_{Hb} (pD 8.2) = 0.249 g/cc; C_{Hb} (pD 8.9) = 0.245 g/cc.

of increased interparticle interaction. The dependence of the measured cross-sections on the surface charge is illustrated in Fig. 3, where data for samples of differing pD but similar Hb concentration are shown.

The cross-sections shown in Figs. 1–3 all were obtained from Hb samples prepared in D_2O buffers. As controls, two H_2O-buffered pH 7.4 samples of relatively high Hb concentration also were examined. The measured cross-section of these samples are shown in Fig. 4. Measurements undertaken to establish the contrast match point for Hb are discussed in Appendix A.

The measured scattering cross-sections were analyzed by using an approach which has been applied successfully in SANS studies of micelle formation by anionic surfactants in aqueous solution (23, 24). The scheme involves calculation of the structure factor, $S'(Q)$, by solving the Ornstein-Zernike equation according to a mean spherical approximation (MSA) (25). The MSA solution is analytical and can be rapidly fit to acquired data by multivariate numerical iteration (26, 27). Scatterers are modeled as monodisperse, charged, hard spheres which interact by a screened Coulomb (Yukawa) potential. The computation of the structure factor is based on the DLVO (Derjaguin, Landau, Verwey, Overbeek) theory of colloidal suspensions (28), in which it is assumed that counterions and co-ions can be treated as point charges whose presence need to be taken into account only insofar as they screen the charge interactions between the macroions. The structure factor of the assembly thus is calculated by a one-component macroion (OCM) theory (17), where the

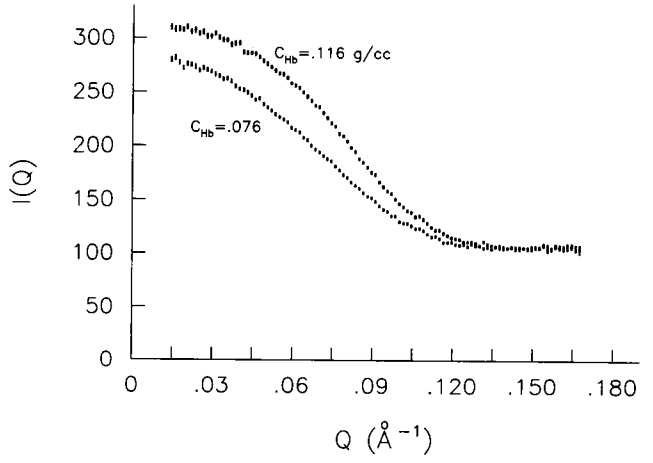

FIGURE 4. Differential neutron scattering cross-sections for HbA in H_2O.

screening due to counterions is accounted for by assuming that the distance between macroions is sufficiently great that the structure of ion "clouds" about a macroion is not influenced by the presence of nearby charged particles, i.e., that the solution is very dilute.

This analysis permits interesting parameters, such as the average surface charge of the macroion, its effective hydrated volume, and the diameter of its equivalent sphere, to be obtained from the fits. A similar procedure has been used in studies of concentrated solutions of bovine serum albumin (15). To facilitate examination of intact native biological vesicles, the data fitting scheme has been modified to provide an additional parameter, namely, the effective solution volume fraction that is occupied by the macroions (12, 29). A slight variation of the program, which sets the Coulomb energy to zero, allows fitting of data to a model of interacting hard spheres. A modification of the theory, that explicitly takes into account the finite sizes and concentrations of the counterions, has been applied (16) to a study of cytochrome *c*, at solution concentrations approaching 20%. The potential used in that treatment yields values for the protein charge that differ slightly from those extracted by the simpler DLVO theory, but the fits to SANS data are equally satisfactory. The present data are fitted by a variant of the simpler theory.

The differential cross-section per unit volume can be written as

$$I(Q) = N_p (\Delta\rho)^2 V_p^2 P(Q) S'(Q), \quad (1)$$

where N_p is the number concentration of protein molecules, V_p is the volume occupied by a single scatterer, and $\Delta\rho = |\rho_{sol} - \rho_p|$ is the 'contrast' (see Appendix A). To account for molecular asymmetry, the particle structure factor $P(Q)$ is taken to be that of an ellipsoid of revolution, viz. (14, 15),

$$P(Q) \equiv \langle F^2 \rangle = \int_0^1 |F(\mu)|^2 \, d\mu, \quad (2)$$

where the form factor $F(\mu)$ is given as:

$$F(\mu) \equiv 3u^{-1} j_1(u) \equiv 3[u^{-2} \sin(u) - u^{-1} \cos(u)], \quad (3a)$$

and $u(\mu)$ is defined by

$$u(\mu) = Q\mathrm{b}\,[(a/\mathrm{b})\mu^2 + (1 - \mu^2)]^{1/2}. \quad (3b)$$

In Eq. 3b, $Q = 4\pi\lambda^{-1} \sin(\theta/2)$ is the Bragg wave number (θ is the scattering angle), and a and b are the lengths of the semimajor and semiminor axes of the prolate ellipsoid of revolution which describes the particle. In Eq. 1, $S'(Q)$ signifies the orientationally averaged interparticle structure factor, defined as

$$S'(Q) = 1 + (\langle F \rangle^2 / \langle F^2 \rangle)\,[S(Q) - 1], \quad (4)$$

where $S(Q)$ is the usual interparticle center–center structure factor defined in terms of the pair distribution function (30). For monomeric Hb, which is presumed to be quasispherical, we take $a/b = 1$, in which case $\langle F \rangle^2 = \langle F^2 \rangle = [3j_1(Qa)/Qa]$, and $S'(Q) = S(Q)$. (We find that our qualitative inferences are unaffected when a and b are taken to have values signifying slight asymmetry.)

When the structure factor is calculated as described in the previous paragraphs (26, 27), the fits of Eq. 1 to the scattering data produce values for the following parameters: *Gek*, a dimensionless surface potential related to Z, the average protein surface charge; $\sigma = 2R$, the effective hard-sphere diameter; η, the volume fraction of the sample which is occupied by the particles; and Amp $= N_p(\Delta\rho)^2 V_p^2$, the scattering amplitude (cf. Eq. 1). To carry out these fits the parameter $A_k \equiv \kappa\sigma$ must be specified, where κ is the Debye length, dependent on the ionic strength of the solution which is usually a known quantity. Unless otherwise noted, A_k was taken to be 6.0 for pD 7.4 data, but was fixed between 1.0 and 3.0 when analyzing pD 8.9 data. The Debye length is calculated according to

$$\kappa = (8\pi e^2 \mathcal{I} \mathcal{N}_A / 10^3 \epsilon k_B T)^{1/2},$$

where $\mathcal{I}$ is the ionic strength, $\mathcal{N}_A$ is Avogadro's number, e is the elemental electronic charge, ϵ is the dielectric constant of the solvent, k_B is Boltzmann's constant, and T is the absolute temperature. *Gek* is defined in terms of these and the above-mentioned variables as

$$Gek = [Z^2 e^2]/\sigma\epsilon k_B T(1 + \kappa/2)^2.$$

The volume fraction of the solution which is occupied by the protein can be estimated independently from direct measurements of the protein concentration. The value then can be used in the fitting procedure as a constrained parameter, as has been done for BSA (15) and cytochrome *c* (16). In doing so, however, it must be recalled that a protein molecule is surrounded by a poorly defined layer of ordered, or 'bound', water which adds to the effective hard sphere radius. The partial specific volume of such "hydrated" particles is represented as

$$\bar{v}_h = \bar{v}_d + w\,\bar{v}_w, \quad (5)$$

where $\bar{v}_d$ is the partial specific volume of the 'bare' protein, w is the weight amount of bound water per weight amount of protein, and $\bar{v}_w$ is the specific volume of water in the solvent. The corresponding "hydrated volume

fraction," η_h, is defined as

$$\eta_h = \bar{v}_h C, \tag{6a}$$

where C is the concentration of bare protein molecules in grams per unit volume. Similarly, the "dry volume fraction," η_d, is designated as

$$\eta_d = \bar{v}_d C. \tag{6b}$$

The SANS instrument which we used has a relatively wide distribution of incident neutron wavelengths ($\delta\lambda/\lambda \approx 0.25$), and the resulting scattering cross-sections are slightly smeared because the measured intensity at a given scattering angle consequently results from a distribution of scattering vectors Q. It is thus necessary to correct fitted values of η and Amp, the adjusted parameters being given in the tables as η_f^c and Amp^c, respectively. Because the corrections are small, it is much simpler to use an empirical procedure to adjust the fitted values, rather than deconvoluting the measured cross-sections before fitting. This procedure is described in Appendix B. In brief, we used a hard-sphere model to generate a set of 'true' differential scattering curves, for several values of η but with $R = \sigma/2$ always taken to be 30.0 Å (representative of the measured values) and Amp taken as the normalized value 1. The curves then were convoluted with a resolution factor $\mathcal{R}(Q|Q')$ according to

$$I_{obs}(Q) = \int \mathcal{R}(Q|Q')\, I(Q')\, dQ', \tag{7}$$

where $\mathcal{R}(Q|Q')$ accounts for geometrical resolution as well as dispersion in neutron wavelength (see Appendix B). The transformed data, $I_{obs}(Q)$, then were fitted, and the resultant values of η, R, and Amp were compared with the values which were used to generate the original 'true' scattering curves. The values of R were essentially unchanged, but variations in η and Amp in some cases were significant. Correction factors necessary to obtain the 'true' values from parameters obtained from the resolution-smeared data are shown in Fig. 5. These correction factors were used to obtain the parameter values reported in the tables.

A comparison of fits to the data given in Fig. 1 for $C = 0.256$ g/cc, obtained by (*a*) constraining the value of η_d to that calculated from Eq. 6b and (*b*) permitting the value of η to float in the fitting procedure, is shown in Fig. 6. The fit obtained using the fixed value of η_d produces an interaction peak which is sharper and shifted to higher Q than the observed data, and is therefore judged to be unacceptable. Increasing the volume fraction to that suggested by Eq. 6a for hydrated particles results in yet poorer fits to the experimental data. Some improvement is noted when a hard sphere model is used, but it still is

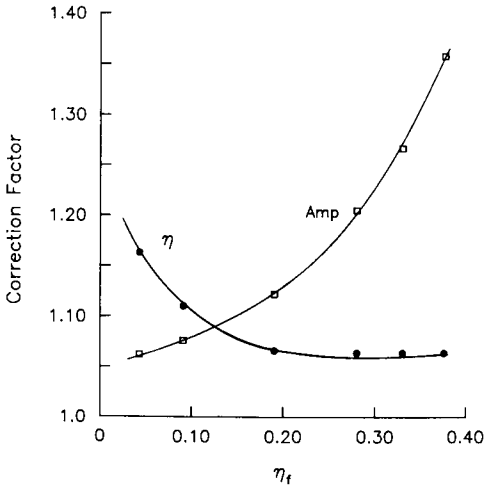

FIGURE 5. Resolution corrections to be applied to inferred values of η and Amp (see text).

impossible to produce good agreement between the calculated and experimental cross-sections. Similar discrepancies are observed for all the Hb solutions, including those that were prepared in H_2O (see Materials). When η is allowed to vary while numerical adjustments of parameters are made, good fits can be achieved (Fig. 6, *solid line*). For these data, the fitted value η_f is 0.176, which is significantly lower than the calculated values $\eta_d = 0.195$ and $\eta_h = 0.273$.

The data shown in Figs. 1–4 therefore were analyzed by permitting the volume fraction η to be an adjustable parameter. For solution conditions near the isoelectric point (pH 7.4), it was found that calculations of the

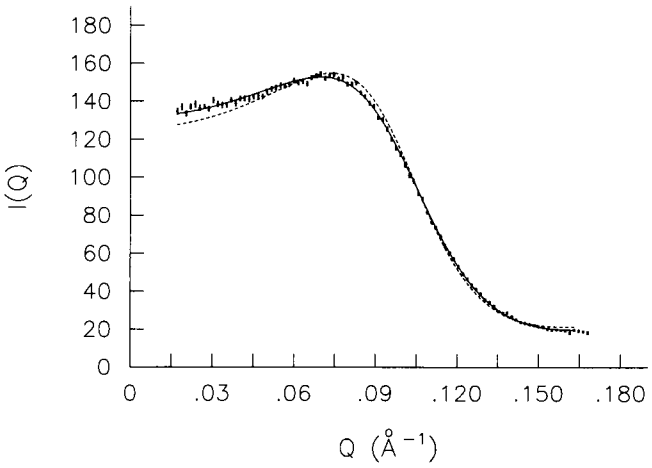

FIGURE 6. Comparison between fitted and measured cross-sections for a typical sample (pD 7.4, $C_{Hb} = 0.256$ g/cc). (*Dotted line*) $\eta = \eta_d = 0.195$. (*Solid line*) $\eta = \eta_f = 0.176$.

structure factor according to a hard sphere potential yield somewhat better fits to the differential scattering cross-sections than do calculations based on the Yukawa potential. Because such fits are easier to implement, the data in Figs. 1–4 were reduced in this manner. The resulting parameters are presented in Tables 1 and 2. Results of similar fits for pD 8.9 samples, based on the curves given in Fig. 4, are summarized in Table 3. In this case the cross-sections were calculated by the full MSA procedure, necessitated by the large surface charge on the molecules and resultant strong intermolecular interactions. Resolution corrections for these data also were carried out by using the procedures described above.

DISCUSSION

When the data in Figs. 1–4 are fitted using a model which assumes monomeric spherical scatterers, the volume fraction of scatterers, η_f^c, required to fit the measured scattering cross-sections is consistently lower than either dry or hydrated volume fractions calculated from the measured hemoglobin concentrations (see Tables 1–3). The relative discrepancy between the fitted value, η_f^c, and the hydrated volume fraction, η_h, expected from the known protein concentration is largest at *low* concentrations, decreasing from over 100% at 0.08 g/cc to ~30% at 0.36 g/cc. The values of $R = \sigma/2$, although slightly larger than expected from the average radius of the hemoglobin molecule, are quite reasonable. However, at high protein concentrations, the fitted amplitudes are significantly smaller than expected. In the discussion which follows, we first consider and discuss the possibility that these results can be explained by uncontrolled processes which altered the samples during the course of the experiments. We then show, by employing theoretical simulations, that it is possible to rationalize the observed effects by postulating the presence of low molecular weight aggregates of hemoglobin. Finally, we compare our results with those of previous studies which might be expected to indicate the existence of such aggregated species.

TABLE 1 Fitted parameters for D_2O solutions, pH 7.4

C	η_d	η_h	η_f^c	$R = \sigma/2$	Amp_{rel}^c
g/cc				*Å*	
0.021	0.015	0.021	—*	29.3	60.5
0.049	0.036	0.050	0.014	28.6	121
0.081	0.059	0.083	0.038	28.6	206
0.153	0.112	0.158	0.090	28.0	333
0.183	0.134	0.188	0.118	27.9	394
0.256	0.194	0.273	0.189	27.5	468
0.356	0.261	0.367	0.290	27.6	622

N.B. η_d, η_h were calculated from Eq 6 with $\bar{v}_d = 0.734$, $w = 0.3$, $\bar{v}_w = 1.0$. Except for the 0.356 g/cc sample, fits were made to a structure factor calculated for a hard-sphere potential because slightly better agreement with experimental data was obtained, as compared with curves determined by the MSA procedure.

*Value fixed at 0, equivalent to the dilute solution limit (Guinier regime).

TABLE 2 Fitted parameters for H_2O solutions, pH 7.4

C	η_d	η_h	η_f^c	$R = \sigma/2$	Amp_{rel}^c
g/cc				*Å*	
0.076	0.056	0.078	0.046	30.4	257
0.116	0.085	0.119	0.076	30.1	370

Possible experimental causes of observed discrepancies

When these studies were begun, it was with the expectation that hemoglobin would provide an example of a quasispherical protein molecule, for which the scattering properties could be calculated using the DLVO theory previously applied to SANS studies of BSA (15) and cytochrome *c* (16). Thus, when the present somewhat unexpected results were obtained, we searched with some care for possible explanations which involved the procedures used to obtain and analyze the data.

One possible explanation for the small fitted values of the *volume fraction* is that the actual volume fraction of protein in solution was, in fact, significantly lower than

TABLE 3 Fitted parameters for D_2O solutions, pH 8.9

C	η_d	η_h	η_f^c	$R = \sigma/2$	Amp_{rel}^c
g/cc				*Å*	
0.021	0.015	0.022	0.015*	30.0	78.2
0.058	0.042	0.059	0.042*	29.7	159
0.071	0.052	0.074	0.037	28.8	202
0.115	0.084	0.118	0.073	28.5	311
0.208	0.153	0.214	0.131	27.8	389
0.245	0.179	0.247	0.158	27.4	484
0.330	0.242	0.340	0.239	26.9	570

*When attempts were made to analyze the lowest concentration samples with the MSA fitting procedure, the program invariably produced a value of η which was less than zero, and the fitting procedure thus self-terminated. Consequently, in these cases the values of η were chosen to be equal to the dry volume fraction, η_d. The fitted amplitudes were found to be independent of A_k and η in these instances. Another fitted parameter, *Gek*, depends sensitively on the choice of A_k. However, A_k is indeterminate for these pD 8.9 samples, which were self-buffering (no added salts). Various values of A_k were chosen during the fitting procedure, and it was observed that the fitted values of η and Amp, in contrast to those of *Gek*, do *not* show significant dependence on the chosen value. For each sample, a best fit was determined by comparing the data points and the calculated curves (χ^2 criterion). The values of A_k giving the best fits thereby were found to be 1.0 for the 0.02–0.12 g/cc samples, and 3.0 for the 0.21–0.33 g/cc samples.

that determined from the measured total concentration of hemoglobin. This could occur because of bulk precipitation of the hemoglobin in D_2O solution, or from the presence of microcrystals or other macroscopic aggregates. The presence of microcrystals ($d \geq 5$ μm) was ruled out by optical examination of the cuvettes subsequent to the scattering experiments, and the presence of a significant concentration of small aggregates was ruled out by near-infrared absorption measurement which showed insignificant turbidity in the samples. (We were particularly concerned about this problem because aggregates were clearly observable in highly concentrated deoxy-HbA samples prepared under similar buffer conditions.) The possibility that errors were made in determining the hemoglobin concentrations also can be ruled out because all samples were measured in duplicate at the conclusion of the scattering experiments, with agreement to within ±2%. Moreover, the concentrations of a number of samples were measured both before and after the scattering experiments, and the agreement between these determinations was better than ±3%. Any contamination with oxidized impurities would decrease the apparent extinction coefficient at the CO peaks and therefore cause the hemoglobin concentrations to be underestimated, rather than overestimated.

Errors in fitting the *amplitudes* of measured cross-sections might occur if the extent of proton exchange between solvent and protein were incorrectly assessed, due either to incomplete deuteration of the protein during dialysis or to dilution of the solvent by slowly exchangeable protons after the samples were loaded into the cuvettes. While these factors might cause an error in the presumed scattering contrast and could affect the amplitudes, they would not influence the measured volume fraction. We assumed that 70% of the exchangeable hydrogen atoms in the main chains, and 100% of those in the side chains, actually are replaced by deuterons, yielding a number close to that (~790) previously inferred experimentally by other SANS measurements on Hb (31). Predicted values of the amplitude (see Appendix A) are much higher than the measured values. Although isotope exchange studies suggest that somewhat fewer than 790 hydrogens are replaced by deuterium (32), the discrepancy between the measured and predicted cross-section amplitudes would not be materially affected by this difference.

Calculated effect of aggregation on scattering cross-sections

The presence of associated species, such as dimers or tetramers of hemoglobin molecules in the concentrated solutions studied in the SANS experiment, could provide an explanation of the results. Such species would shift the apparent interaction peak of the structure factor, because both the particle sizes and the interparticle distances would be larger than for an equivalent solution of monomers. On average the scattering from the larger particles would occur into smaller values of Q. As a result, if the structure factor were modeled by assuming that only monomers are present, the inferred volume fraction would be smaller than that calculated from the equivalent monomer concentration. In order to quantitate this intuitive expectation (i.e., that polydispersity produced by aggregation of hemoglobin tetramers could mimic the observed deviations between the measured cross-sections and those predicted for monomeric scatterers), cross-sections for polydisperse systems were simulated and then fitted using the same procedure which was used to analyze the experimental data.

Unfortunately no general method to account for polydispersity currently is available. Exact analytical expressions for the structure factor of polydisperse *hard-sphere* fluids have been obtained (33, 34), but their complicated mathematical form reduces their usefulness in fitting cross-section data. Analytical expressions for averaged structure factors, which can be used to fit SANS data, have been derived in two different cases by using a decoupling approximation (23, 35); in both instances the expressions are in qualitatively good agreement with those of the true hard-sphere model, even at relatively high volume fractions (34). We used one of these approximations (23) to generate hypothetical structure factors for a number of assumed aggregate distributions. In doing so, analogues of Eqs. 1 and 4 were employed but, instead of the true polydisperse structure factor, an approximate $S(Q)$ was calculated by assuming monodisperse particles having an equivalent (average) hard sphere diameter $\bar{\sigma}$ given as (23):

$$\bar{\sigma}^3 = \sum_i^n \beta_i \sigma_i^3, \tag{8}$$

with $\beta_i = \eta_i/\eta$, which represents the contribution to the total volume fraction due to all particles of type i. Effective diameters σ_i were defined as

$$\sigma_i = 2(a_i b_i^2)^{1/3}, \tag{9}$$

where the a_i and b_i are the major and minor semiaxes of the particles. The terms $\langle F^2 \rangle$ and $\langle F \rangle^2$ in Eq. 4 were modified to account for polydispersity by setting

$$\langle F^2 \rangle = \sum_{i=1}^n \alpha_i \langle F_i^2 \rangle, \quad \langle F \rangle^2 = \sum_{i=1}^n \alpha_i \langle F_i \rangle^2. \tag{10}$$

F_i is the form factor of the ith particle and $\alpha_i = N_i(\Delta\rho)^2 V_i^2$ is the fraction of the total scattering amplitude contributed by particles with diameter σ_i, normalized such that $\sum \alpha_i = 1$. α_i is related to β_i as $\alpha_i = \beta_i \sigma_i^3/\bar{\sigma}^3$. We

note that Eq. 4 is not rigorous in the limit $Q \rightarrow 0$ for hard-sphere systems, but it is acceptably accurate near the first diffraction peak (34).

We used this procedure to calculate scattering cross-sections for a number of systems which were assumed to contain four discrete particle sizes: monomers (i.e., the $\alpha_2\beta_2$ HbA tetramer), dimers, octamers, and oligomers composed of 16 monomers (16-mers). Dimensions of the particles were taken to be $R_1 = \sigma_1/2 = a = b = 28$ Å for monomers; $a = 56$ Å, $b = 28$ Å ($a/b = 2$), with an equivalent radius of $R_2 = (ab^2)^{1/3} = 35$ Å, for dimers; $R_3 = a = b = 56$ Å for octamers; and $a = 112$ Å, $b = 56$ Å, $R_4 = (ab^2)^{1/3} = 71$ Å, for 16-mers. Cross-sections were calculated according to Eqs. 8–10 for this system of particles, using the full MSA procedure (with values $A_k = 6$ and $Gek = 0.001$, which approximates a hard sphere model). The calculated cross-section in Figs. 7 and 8 show the anticipated effects: the interaction peak shifts to smaller values of Q and the scattered amplitudes decrease monotonically with increasing scattering fractions α_i of the aggregated species. The fits to the calculated data, when only monomers and dimers are present, are shown as the dotted and/or dashed lines in Fig. 7, *a* and *b*, and the parameters obtained are summarized in Table 4. The fits are quite good and, as anticipated, the fitted values for η_f and amplitude both decrease monotonically with increasing fraction of dimer. The fitted values of the equivalent monomeric interaction parameter, *Gek* (not shown), differ from the assumed value but are low, indicating an almost uncharged surface. The calculated effect of aggregation on the scattering cross-section seemingly is much less dramatic at low volume fractions, in that the assumed monomer model is better able to fit the calculated curves when the actual volume fraction is 0.1 (Fig. 7 *a*) than when the volume fraction is 0.3 (Fig. 7 *b*); however, it should be stressed that *relative* discrepancies between actual and calculated volume fractions are greater at low volume fractions (see Table 4).

If the solid lines in Fig. 7 represented real scattering data, the fits obtained by assuming monomeric scatterers would be close to acceptable, particularly if the experimental uncertainties in the data points were included. Although the quality of the fits becomes poorer as the percentage of dimers increases, one nonetheless could be misled into believing that the assembly is composed only of monomers, except for the fact that the apparent volume fraction, η_f, is considerably less than the "true" value. Even if the sample were to consist entirely of dimers, the fitted value of R (upon assuming that the scattering molecules were spherical monomers), while high, would not be unreasonable (Table 4). Similar effects are observed in calculations in which octamers and/or 16-mers are assumed to be present (Fig. 8). In these cases, the

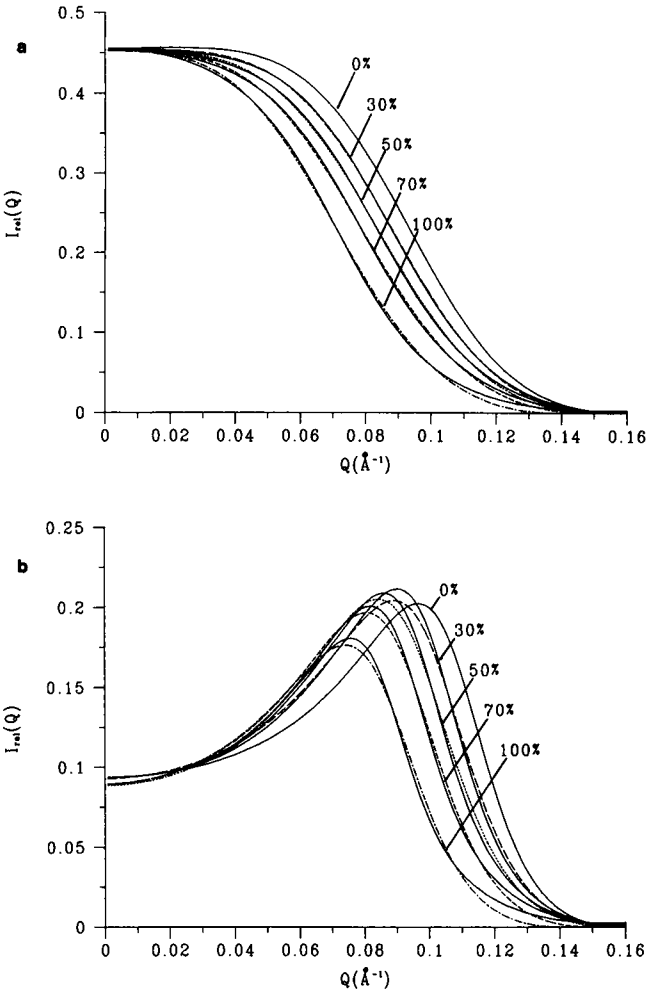

FIGURE 7. Model calculations (*solid line*) of systems of polydisperse molecules consisting only of monomers and dimers. Corresponding dotted/dashed lines represent the best fits to the models, assuming the systems are monodisperse. (——) 100% monomer; (— —) 70% monomer, 30% dimer; (---) 50% monomer, 50% dimer; (– – –) 30% monomer, 70% dimer; (———) 100% dimer. (*a*) Volume fraction, $\eta = 0.1$. (*b*) Volume fraction, $\eta = 0.3$.

apparent volume fraction, η_f, and the amplitude are both reduced. In addition, the fitted value of the apparent radius increases (for the curves in Fig. 8, the fitted values of R are found to be ≥ 40 Å when the distribution of monomer, dimers, octamers, and 16-mers is 25, 25, 25, and 25%, respectively). Nonetheless, in many instances good fits can be obtained. However, in all cases when the true volume fraction is used as a *fixed* parameter, large differences occur between the fitted and "true" cross-section curves.

These model calculations suggest that the presence of high-order oligomers could cause differences between the

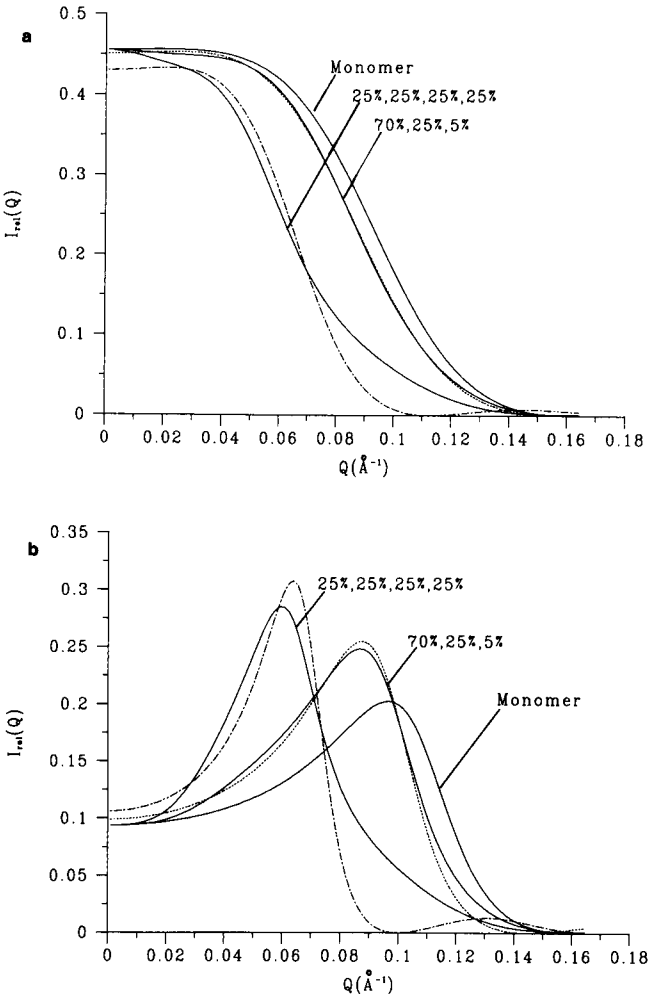

FIGURE 8. Model calculations (*solid lines*) of systems of polydisperse molecules consisting of monomer, dimers, octamers, and 16-mers. Corresponding dotted/dashed lines represent the best fits to the models, assuming the systems are monodisperse. Key: (—) 100% monomer; (–·–·) 25% each monomer, dimer, octamer, 16-mer; (---) 70% monomer, 25% dimer, 5% 16-mer. (*a*) Volume fraction, $\eta = 0.1$. (*b*) Volume fraction, $\eta = 0.3$.

calculated and measured $I(\mathbf{Q})$ which are similar to those observed for the experimental data. We, therefore, conclude that it would be possible to explain the observed cross-sections at any single concentration and set of solvent conditions by assuming that the solution contains a volume fraction of dimers or other small oligomers. However, due to the approximate nature of the model calculations, and the possible degeneracy of the calculated cross-sections (i.e., different mixes of particle sizes might yield quite similar cross-sections when interactions are present), it is not possible to quantitate the degree of polydispersity from the measured cross-section.

TABLE 4 Analyses of simulated scattering from mixtures of monomers and dimers

% Dimer	η	η_f	η/η_f	$R = \sigma/2$	Relative Amp (fitted)
				Å	
0	0.1	0.1	1.0	28.0	1.0
30	0.1	0.084	0.84	28.6	0.90
50	0.1	0.071	0.71	29.2	0.83
70	0.1	0.056	0.56	29.9	0.75
100	0.1	0.043	0.43	32.0	0.70
0	0.3	0.3	1.0	28.0	1.0
30	0.3	0.266	0.89	28.7	0.91
50	0.3	0.236	0.79	28.9	0.80
70	0.3	0.238	0.79	30.1	0.78
100	0.3	0.221	0.74	31.9	0.67

Comparison with other methods

Given the result that limited aggregation could explain the observed scattering cross-sections, it is important to ask whether the presence of such aggregates can provide a self-consistent explanation for all of the experimental results.

At first glance, the results in Tables 1–3 provide little obvious support for the usual notion that a simple equilibrium process is taking place to produce dimers or higher aggregates. Although estimation of the dependence on concentration of the mole fraction of aggregates is complicated by the nonideality of concentrated hemoglobin solutions, one would predict that the amount of hemoglobin present in the form of dimers would increase as the protein concentration increases. For example, if the mole fraction of dimerized hemoglobin were 10% at a concentration of 0.05 g/cc, that value would be expected to increase to above 80% at a concentration of 0.3 g/cc (36). However, the fitted mole fractions are actually in better agreement with the actual values at *higher* concentrations, in that the *relative* difference in the fitted and measured volume fractions is nearly 100% at concentrations of 0.05–0.08 g/cc, decreasing to below 30% at concentrations above 0.3 g/cc (Fig. 9 *a*). The opposite behavior is true for the amplitudes, which seem to be in better agreement at low concentrations (Fig. 9 *b*). In this respect, the data are in accord with the results in Table 4, which show that the fitted volume fraction is more sensitive to the presence of dimers at low concentrations.

Limited evidence for the presence of such aggregates also is obtained from other experiments. As mentioned in the Introduction, quasielastic light scattering studies in isolated single cells have been interpreted as indicating the presence of Hb aggregates (11). Possible support for molecular associations also is obtained from studies of

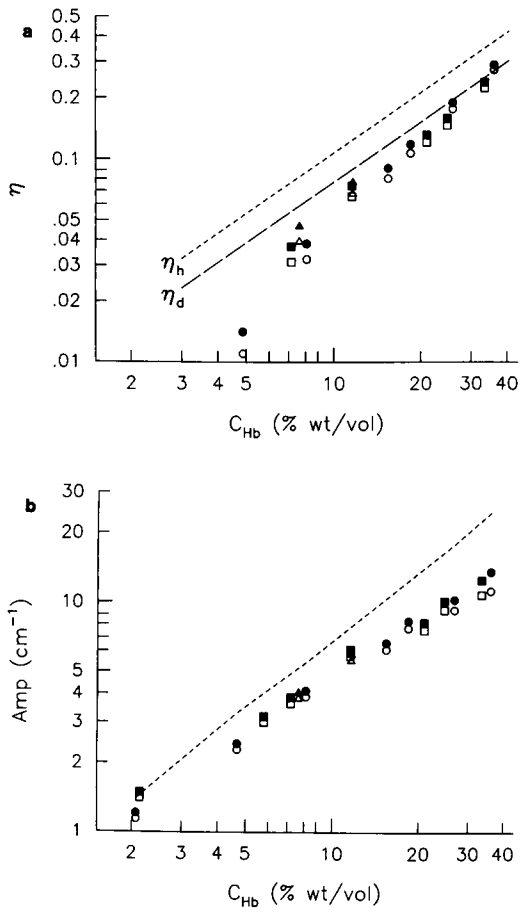

FIGURE 9. Fitted values of η and Amp (*open symbols*), and values after being corrected for resolution (*solid symbols;* see Fig. 6). (*Circles*) pD 7.4, D_2O; (*squares*) pD 8.9, D_2O; (*triangles*) pH 7.4, H_2O. (*a*) Fitted values of volume fraction, η_f. Dotted lines correspond to calculated volume fractions (see text). (*b*) Fitted values of amplitude, Amp. Dotted line corresponds to expected values of Amp for D_2O solutions (see Appendix A). Scattering amplitudes for D_2O samples were put on an absolute scale by comparing with data obtained from a known silica gel standard. Data for the H_2O samples (*triangles*) were put on a *relative* scale by fitting the expected H_2O amplitudes to the corresponding values of D_2O.

molecular rotational correlation times measured by nuclear magnetic resonance (37) and electron paramagnetic resonance (EPR) (38) techniques. The rotational correlation time is related to the time necessary for randomization of hemoglobin molecule orientations by Brownian motion, which depends on particle size and solution viscosity. A fivefold increase in rotational correlation time is observed when the Hb concentration is increased from 5 to 36 weight percent for both oxy- and carboxy-Hb (37, 38). In both the EPR and NMR studies, the reciprocal correlation time was found to decrease linearly with hemoglobin concentration for HbA, suggesting that most of the observed increase arises from the increase in solution viscosity which accompanies the increase in protein concentration. However, in the case of carbonmonoxy hemoglobin S in aqueous buffer, a quadratic component was observed and attributed to dimer formation (38). It is possible that the change from H_2O to D_2O promotes a similar process in HbA.

Fixed-angle quasielastic light scattering studies (at 90°) of oxy-HbA solutions at pH 7.4 also show features which might indicate molecular associations (39). A sensitive measure of size heterogeneity in noninteracting systems of scatterers is the variance (i.e., dispersion) in the value of the particle diffusion coefficient, obtained from the cumulants of the measured autocorrelation function. By this criterion, oxy-HbA pH 7.4 solutions have been found to be quite heterogeneous (39), with the apparent heterogeneity increasing markedly as the amount of Hb is decreased. This interpretation of the light scattering results would suggest that aggregates are present even at relatively low Hb concentrations.

In contrast, analyses of a variety of thermodynamic and hydrodynamic measurements which had been made on concentrated hemoglobin solutions (2–6) argue against the likehood of any significant aggregation if the Hb concentration is below 0.30 g/cc (7–10). Additionally, it was inferred that the only interaction between hemoglobin molecules which needs to be included in aqueous solution near isoelectric pH is the hard-sphere excluded volume interaction (7–10). Those interactions produce activity coefficients which have been used to fit sedimentation equilibrium, osmotic pressure, diffusion coefficient, and viscosity data at concentrations up to 40% by weight with no additional terms. Expressions based on the model were fit to previously published data and reasonably consistent results were obtained (8, 9); however, no attempt was made to see whether the data could be equally well fit by equivalent thermodynamic models which assume polydispersity, nor were upper limits put on the mole fraction of dimers or other aggregates.

Also, average mutual diffusion coefficients deduced from photon autocorrelation functions for both oxy- and carboxy-HbA at the isoelectric point (pH 6.9) decrease linearly with increasing concentration (40, 41). Such observations have been interpreted by using theories (developed for low particle densities) which account for increased hydrodynamic and electrostatic intermolecular interactions as the concentration increases, without involving any aggregation of hemoglobin tetramers. For these solution conditions, the variance in the data, as determined from higher-order cumulants, increases markedly when the Hb concentration exceeds 20%, possibly indicating aggregate formation; because the mean diffusion coefficient is insensitive to the presence of a small amount of particle dimers, it was noted that associated or aggre-

gated Hb thus could comprise up to 30% of the mass of the scattering assembly (40). However, these and other (42) dynamic light scattering studies failed to show evidence of Hb dimers or higher-order aggregates when the Hb concentration was less than ~0.20 g/cc.

II conclusion, a plausible explanation of cross-sections produced by small-angle neutron scattering from carboxy-HbA solutions is the formation of small oligomers of tetrametic HbA. It is clear, though, that discrepancies observed by fitting SANS data to assumed monomeric Hb distributions have not yet been conclusively resolved. There is some uncertainty, too, in the interpretation of data obtained by other techniques. In many instances, effects arising from aggregation are easily masked by those due to hydrodynamic interactions. When comparing the results of our studies with those obtained from viscosity, dynamic light scattering, and similar techniques, it should be kept in mind that SANS cross-sections represent the superposition (ensemble average) of instantaneous 'snap-shots' of a system, and may detect the presence of transient bonding that is not readily discernible by other physical techniques. With proper interpretation, diffraction measurements may provide a clearer image of transitory, weak, molecular associations than can be obtained by other methods. However, quantitative interpretation of scattering data from heterogeneous assemblies will require the development of appropriate theoretical models and data-fitting procedures.

APPENDIX A: CALCULATION OF ABSOLUTE SCATTERING AMPLITUDES

Data are placed on an absolute scale by calibrating against scattering from a standard silica gel sample, measured under the same experimental conditions. The absolute amplitudes are calculated from

$$A\,(\mathrm{cm}^{-1}) = \frac{A\,(\mathrm{rel})}{A_s\,(\mathrm{rel})}\frac{t_s}{t}\frac{d_s}{d}\frac{T_s}{T}A_s\,(\mathrm{cm}^{-1}), \qquad \text{(A1)}$$

where the subscript, S, refers to the silica standard. In Eq. A.1, A (cm^{-1}) and A (rel) are the absolute and relative amplitudes, respectively, t is the counting time, d is the neutron path length, and T is the sample transmission. The absolute amplitude of the silica standard is taken to be A_S (cm^{-1}) = 32.0 ± 1.5 cm^{-1}, which was obtained from previous measurements against vanadium as a primary standard.

The measured absolute amplitudes can be compared to those calculated based solely on the properties of the molecule. Written in terms of the concentration, C, molecular weight, M_w, total neutron scattering length, Σb, and partial specific volume, $\bar{v}$, the absolute amplitudes are calculated from

$$A\,(\mathrm{cm}^{-1}) = C N_A M_w\left[\frac{\Sigma b}{M_w} - \frac{\rho_s \bar{v}}{N_A}\right]^2, \qquad \text{(A2)}$$

where ρ_s is the scattering length density of the solvent and N_A is Avogadro's number. For the calculations, the measured values of C, in grams per cubic centimeter, were used, M_w was taken as 64,500, and $\bar{v}$ was assumed to be 0.735 g/cc. The total scattering length, Σb, was calculated directly from the amino acid composition of HbA. For molecules in D_2O solvent, the effects of H-D exchange were calculated by assuming that 70% of the exchangeable hydrogen atoms in the main chains and 100% in the side chains actually did exchange with deuterium atoms in the solvent.

The bracketed quantity appearing in Eq. A2 is zero at the "contrast match point," i.e., when the scattering length ρ_s has been appropriately adjusted by varying the percentage of D_2O in the solvent. From Eq. A2, it is apparent that $[I(0)]^{1/2}$, normalized for sample concentration, should vary as

$$\pm[I(0)]^{1/2} \sim \frac{\Sigma b}{M_w} - \frac{\rho_s \bar{v}}{N_A}. \qquad \text{(A3)}$$

Contrast variation data, expressed in this way, indicate a match point (~39% D_2O) which is close to a value reported previously for Hb (32).

APPENDIX B: RESOLUTION CORRECTIONS

The measured scattering intensity, $I_{obs}(Q)$, can be represented by a convolution of the theoretical scattering function, $I(Q)$, with the instrumental resolution function (43). For the SANS instrument at the National Institute of Standards and Technology the resolution function itself is a convolution of the geometrical resolution function, $U(Q)$, with the wavelength resolution function, $W(x)$, where $x = \lambda'/\lambda$ (Berk, N. F., unpublished observation). Using the above notation, $I_{obs}(Q)$ is written as

$$I_{obs}(Q) = \int U(Q - xQ')\,W(x)\,I(Q')\,dQ'\,dx. \qquad \text{(B1)}$$

The geometrical resolution function, $U(Q)$, can be represented in the standard form for pinhole collimation by a detector function, $D(Q)$, and a neutron beam profile function, $B(Q)$, as

$$U(Q) = \int D(Q - Q')\,B(Q')\,dQ'. \qquad \text{(B2)}$$

The beam profile function, $B(Q)$, is represented by a modified Bessel function of the first kind. The detector function, $D(Q)$, is a gaussian with a width of σ_Q, where σ_Q^2 is the variance in the value of Q (20). Only the terms due to the angular divergence of the neutron beam are used to define σ_Q^2, because the wavelength dependence is treated in the separate function $W(x)$, which is unique to the NIST SANS instrument. $W(x)$ is represented by a triangular function with a Maxwellian tail (Berk, N. F., unpublished).

Estimates of the resolution corrections to the hemoglobin data were obtained by first calculating model scattering intensities, $I(Q)$, assuming spherical particles for $P(Q)$, and hard-sphere interparticle interactions for $S'(Q)$. A radius of 30 Å, background of 0.0, and an amplitude of 1.0 were chosen for the particles in all cases. The volume fraction, η, was chosen between 0.1 and 0.4 to mimic the full range of experimental η values.

The calculated model scattering intensities were smeared, using the above convolution integrals, to model $I_{obs}(Q)$. These "smeared" curves were then fit, using the spherical form of $P(Q)$ and assuming hard sphere interactions for $S'(Q)$. In initial fits, the particle radius was a variable parameter. However, because the fitted radii were very close to the original value of 30 Å, the radius was held fixed at this value for the final fits. Thus, only the background, the amplitude, and the volume fraction, η, remained as fitted parameters.

The parameters obtained by fitting to the "smeared" curves were compared with those used to generate the model curves to determine the magnitude of the change on each parameter due to resolution effects (see Fig. 5). The values of Amp and η_f obtained from fits to the hemoglobin data (presented in Tables 1–3) then were adjusted accordingly (see

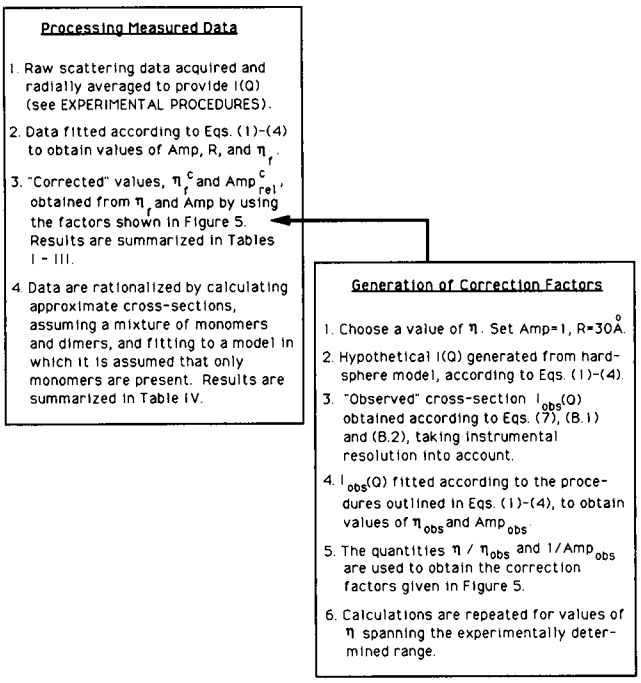

FIGURE 10. Summary of procedures used to fit measured scattering cross-sections and to analyze data.

summary, Fig. 10). This indirect method was chosen over the more direct method of including the convolution integrals in the data fitting program to avoid prohibitive data fitting times.

Received for publication 20 November 1989 and in final form 27 April 1990.

REFERENCES

1. Adair, G. S. 1928. A theory of partial osmotic pressures and membrane equilibria, with special reference to the application of Dalton's Law to hemoglobin solutions in the presence of salt. *Proc. R. Soc. London Ser. A.* 120:573–603.
2. Williams, R. C., Jr. 1973. Concerted formation of the gel of hemoglobin S. *Proc. Natl. Acad. Sci. USA.* 70:1506–1508.
3. Briehl, R., and S. Ewert. 1974. Effects of pH, 2,3-diphosphoglycerate and salts on the gelation of sickle cell deoxyhemoglobin. *J. Mol. Biol.* 80:445–458.
4. Chien, S., S. Usami, R. J. Dellenback, and C. A. Bryant. 1971. Comparative hemorheology-hematological implications of species differences in blood viscosity. *Biorheology.* 8:35–57.
5. Keller, K. H., E. R. Canales, and S. I. Yum. 1971. Tracer and mutual diffusion coefficients of proteins. *J. Phys. Chem.* 75:379–387.
6. Riveros-Moreno, V., and J. B. Wittenberg. 1972. The self-diffusion coefficients of myoglobin and hemoglobin in concentrated solutions. *J. Biol. Chem.* 247:895–901.
7. Minton, A. P., and P. D. Ross. 1978. Concentration dependence of the diffusion coefficient of hemoglobin. *J. Phys. Chem.* 82:1934–1938.
8. Ross, P. D., and A. P. Minton. 1977. Analysis of non-ideal behavior in concentrated hemoglobin solutions. *J. Mol. Biol.* 112:437–452.
9. Ross, P. D., R. W. Briehl, and A. P. Minton. 1978. Temperature dependence of nonideality in concentrated solutions of hemoglobin. *Biopolymers.* 17:2285–2288.
10. Minton, A. P. 1983. Thermodynamic nonideality and dependence of partition coefficient upon solute concentration in exclusion chromatography. II. An improved theory of equilibrium partitioning of concentrated protein solutions. Application to hemoglobin. *Biophys. Chem.* 18:139–143.
11. Nishio, I., J. Peetermans, and T. Tanaka. 1985. Microscope laser light scattering spectroscopy of single biological cells. *Cell Biophys.* 7:91–105.
12. Krueger, S., and R. Nossal. 1988. SANS studies of interacting hemoglobin in intact erythrocytes. *Biophys. J.* 53:97–105.
13. Tischler, R. B., and F. D. Carlson. 1987. Qausi-elastic light scattering studies of membrane motion in single red blood cells. *Biophys. J.* 51:993–997.
14. Bendedouch, D., and S.-H. Chen. 1983. Structure and interparticle interactions of bovine serum albumin in solution studied by small-angle neutron scattering. *J. Phys. Chem.* 87:1473–1477.
15. Nossal, R., C. J. Glinka, and S.-H. Chen. 1986. SANS studies of concentrated protein solutions. I. Bovine serum albumin. *Biopolymers.* 25:1157–1175.
16. Wu, C.-F., and S.-H. Chen. 1987. SANS studies of concentrated protein solutions: determinations of the charge, hydration, and H/D exchange in cytochrome c. *J. Chem. Phys.* 87:6199–6205.
17. Hayter, J. B., and J. Penfold. 1981. An analytic structure factor for macroion solutions. *Mol. Phys.* 42:109–118.
18. Bendedouch, D., S.-H. Chen, and W. C. Koehler. 1983. Determination of interparticle structure factors in ionic micellar solutions by small angle neutron scattering. *J. Phys. Chem.* 87:2621–2628.
19. Glascoe, P. K., and F. A. Long. 1960. Use of glass electrodes to measure acidities in deuterium oxide. *J. Phys. Chem.* 64:188–190.
20. Glinka, C. J., J. M. Rowe, and J. G. LaRock. 1986. The small-angle neutron scattering spectrometer at the National Bureau of Standards. *J. Appl. Crystallogr.* 19:427–439.
21. Glinka, C. J., and N. F. Berk. 1983. The two-dimensional PSD at the National Bureau of Standards' small angle neutron scattering facility. *In* Position-Sensitive Detection and Thermal Neutrons. P. Convert and J. B. Forsyth, editors. Academic Press, Inc., New York. 141–148.
22. Chen, S.-H., and D. Bendedouch. 1986. Structure and interactions of proteins in solutions studied by small angle neutron scattering. *Methods Enzymol.* 130:79–116.
23. Kotlarchyk, M., and S.-H. Chen. 1983. Analysis of small angle neutron scattering spectra from polydisperse interacting colloids. *J. Chem. Phys.* 79:2461–2469.
24. Kotlarchyk, M., S.-H. Chen, J. S. Huang, and M. W. Kim. 1984. Structure of three-component microemulsions in the critical region determined by small-angle neutron scattering. *Phys. Rev. A.* 29:2054–2069.
25. Waisman, E., and J. L. Lebowitz. 1972. Mean spherical model integral equation for charged hard spheres. I. Method of solution. *J. Chem. Phys.* 56:3086–3093.
26. Hansen, J.-P., and J. B. Hayter. 1982. A rescaled MSA structure factor for dilute charged colloidal dispersions. *Mol. Phys.* 46:651–656.
27. Lin, T. S., S.-H. Chen, N. E. Gabriel, and M. F. Roberts. 1986. Use

of small-angle neutron scattering to determine the structure and interaction of dihexanoylphosphatidylcholine micelles. *J. Am. Chem. Soc.* 108:3499–3507.

28. Verwey, E. J. W., and J. Th. G. Overbeek. 1948. Theory of the Stability of Lyophobic Colloids. Elsevier, New York.
29. Krueger, S., J. W. Lynn, J. T. Russell, and R. Nossal. 1989. Small angle neutron scattering method for *in situ* studies of the dense cores of biological cells and vesicles: applications to isolated neurosecretory vesicles. *J. Appl. Crystallogr.* 22:546–555.
30. Egelstaff, P. A. 1967. An Introduction to the Liquid State. Academic Press, Inc., New York.
31. Schelten, J., P. Schlecht, W. Schmatz, and A. Mayer. 1972. Neutron small angle scattering of hemoglobin. *J. Biol. Chem.* 247:5436–5441.
32. Ray, J., and S. W. Englander. 1986. Allosteric sensitivity in hemoglobin at the α-subunit N-terminus studied by hydrogen exchange. *Biochemistry.* 25:3000–3007.
33. Vrij, A. 1979. Mixtures of hard spheres in the Percus–Yevick approximation. Light scattering at finite angles. *J. Chem. Phys.* 71:3267–3270.

33a. van Beurten, P., and A. Vrij. 1981. Polydispersity effects in the small-angle scattering of concentrated solutions of colloidal spheres. *J. Chem. Phys.* 74:2744–2748.

34. Griffith, W. L., R. Triolo, and A. L. Compere. 1987. Analytical scattering function of a polydisperse Percus–Yevick fluid with Schulz-(Γ-) distributed diameters. *Phys. Rev. A.* 35:2200–2206.
35. Chen, S.-H., and M. Kotlarchyk. 1986. Surfactants in Solution. K. L. Mittel, editor. Plenum Publishing Co., New York.
36. Minton, A. P. 1981. Excluded volume as a determinant of macromolecular structure and reactivity. *Biopolymers.* 20:2093–2120.
37. Lindstrom, T. R., S. H. Koenig, T. Boussios, and J. F. Bertles. 1976. Intermolecular interactions of oxygenated sickle hemoglobin molecules in cells and cell-free solutions. *Biophys. J.* 16:679–689.
38. Johnson, M. E., and S. S. Danyluk. 1978. Spin label detection of intermolecular interactions in carbonmonoxy sickle hemoglobin. *Biophys. J.* 24:517–524.
39. LaGattuta, K. J., V. S. Sharma, D. F. Nicoli, and B. K. Kothari. 1981. Diffusion coefficients of hemoglobin by intensity fluctuation spectroscopy. *Biophys. J.* 33:63–80.
40. Jones, C. R., C. S. Johnson, Jr., and J. T. Penniston. 1978. Photon correlation spectroscopy of hemoglobin: diffusion of oxy-HbA and oxy-HbS. *Biopolymers.* 17:1581–1593.
41. Hall, R., Y. S. Oh, and C. S. Johnson, Jr. 1980. Photon correlation spectroscopy in strongly absorbing and concentrated samples with applications to unliganded hemoglobin. *J. Phys. Chem.* 84:756–767.
42. Veldkamp, W. B., and J. R. Votano. 1976. Effects of intermolecular interaction on protein diffusion in solution. *J. Phys. Chem.* 80:2794–2801.
43. Moore, P. B. 1980. Small-angle scattering. Information content and error analysis. *J. Appl. Crystallogr.* 13:168–175.